Acta Materialia 129 (2017) 112–123

Contents lists available at ScienceDirect

Acta Materialia

journal homepage: www.elsevier.com/locate/actamat

Full length article

Nucleation of recrystallisation in castings of single crystal Ni-based superalloys

Harshal N. Mathur, PhD [a], Chinnapat Panwisawas, PhD [b], C. Neil Jones, PhD [c], Roger C. Reed, PhD [d], Catherine M.F. Rae, DPhil [a, *]

[a] Department of Materials Science and Metallurgy, Cambridge University, 27 Charles Babbage Road, Cambridge, CB3 0FS, United Kingdom
[b] School of Metallurgy and Materials, College of Engineering and Physical Science, The University of Birmingham, Edgbaston, Birmingham, B15 2TT, United Kingdom
[c] Rolls-Royce plc, PO Box 31, Derby, DE24 8BJ, United Kingdom
[d] Department of Materials, University of Oxford, Parks Road, Oxford, OX1 3PH, United Kingdom

ARTICLE INFO

Article history:
Received 22 December 2016
Received in revised form
18 February 2017
Accepted 20 February 2017
Available online 28 February 2017

Keywords:
Recrystallisation
Nucleation
Investment casting
Single-crystal Ni superalloys

ABSTRACT

Recrystallisation in single crystal Ni-based superalloys during solution heat treatment results in a significant cost to the investment casting industry. In this paper two sources of surface nucleation have been identified in the alloy CMSX-4®. Firstly, Electron Backscattered Diffraction (EBSD) has revealed micro-grains of γ′, between 2 and 30 μm diameter in the layer of surface eutectic found in the upper part of the casting. These have high angle boundaries with respect to the bulk single crystal and a fraction coarsen during solution heat treatment. Secondly, in the lower regions where surface eutectic does not form, locally deformed regions, 5–20 μm deep, form where the metal adheres to the mould. The local strain causes misorientations up to ≈20° with respect the bulk single crystal, and after heat treatment these regions develop into small grains of similar low-angle misorientations. However, they also form twins to produce further grains which have mobile high-angle boundaries with respect to the bulk single crystal. Experiments have shown that micro-grains at the surface grow to cause full recrystallisation where there is sufficient strain in the bulk material, and by removing these surface defects, recrystallisation can be completely mitigated. Etching of the cast surface is demonstrated to be an effective method of achieving this.

1. Introduction

The occurrence of recrystallisation in single crystal superalloy components during the solutioning heat treatment has long posed a significant mystery: how do you nucleate mobile high angle boundaries in a single-crystal material undergoing very moderate strains? In the past investigations have focussed on the strain necessary to drive the migration of boundaries [1–3], but avoid this central issue. The nucleation of recrystallisation is normally associated with the migration of existing boundaries experiencing a significant local difference in dislocation density on either side [4–6]. In the absence of grain boundaries, severe deformation of 20–25% by, for example, indentation [3,7–10] or compression [11–13] is required to trigger recrystallisation, often magnified by the presence of strain concentrators such as carbides [14]. Recrystallisation has also been observed during thermo-mechanical fatigue, nucleating at the intersection of deformation twin bands [15,16]. None of these possibilities arises in cast single crystal superalloys where potential strains are low and carbides are absent by design. Nucleation is always at, or very close to, the cast surface [17], but is unlikely to occur spontaneously. This work, for the first time, provides evidence of viable nuclei in the surface layers of single crystal castings and demonstrates that under suitable conditions of very moderate strain these can develop into sizable grains equipped with mobile high angle boundaries.

2. Background

Single crystal superalloy components are vulnerable to grain boundaries as the elements strengthening grain boundaries are removed to give a more effective solution heat treatment. Boundary misorientation angles above 10° lead to a catastrophic drop in creep

* Corresponding author.
E-mail address: cr18@cam.ac.uk (C.M.F. Rae).

http://dx.doi.org/10.1016/j.actamat.2017.02.058

rupture life [18]. Grain boundaries act as crack initiation and propagation sites during creep deformation and lead to a significant reduction in the creep rupture life following recrystallisation [18–22]. Fatigue crack nucleation and propagation rates are also higher in recrystallised samples, [23,24]. Hence, any sign of recrystallsation, or indeed the inability to examine a casting through, for example, the formation of surface scale [25], results in the rejection of the components and a significant increase in cost. Recrystallisation also constrains component design, since complex geometries are more prone to developing higher local casting strains [1,2,13]. Furthermore, work by Hill [26] has shown that the susceptibility to recrystallisation depends on the alloy composition; the critical strain for recrystallisation was nearly halved for some recrystallisation-prone alloys, which thus become uneconomic despite other good properties.

Recrystallisation is driven by the strains induced from the different thermal response of the mould and the casting. It is a complex function of the material expansion coefficients and modulae, the component design and the casting process parameters. Quantifying the threshold strain to propagate recrystallisation following nucleation is not straightforward as the dislocation density is not a monotonic function of strain and the dislocation configuration and stored energy depends on the deformation temperature [1,27]. However, observations of the deformation in castings prior to heat treatment show that the dislocation configurations most closely resemble those produced at high temperatures, demonstrating that the majority of the strain is induced during the very early stages of cooling after solidification [1]. By applying the solution heat treatment to samples deformed to known strains at these temperatures the critical strain to fuel recrystallisation has been identified at 1–2% [1,2] in agreement with previous work [3]. Modelling of the strains induced during cooling has demonstrated that in specific locations the metal can experience sufficient stress to induce the plastic deformation necessary for recrystallisation, and experimental castings of various geometries have validated this modelling [1,2]. One strategy to control recrystallisation is to reduce deformation during cooling by changing the ceramic mould and core materials, reducing the strength of the mould, but increasing the risk of failure or distortion. An alternative approach is to eliminate or reduce the nucleation of recrystallsation.

3. Experimental

3.1. Materials

CMSX 4,[1] a second-generation superalloy (composition given in Table 1) was cast parallel to [001] under conditions consistent with normal foundry production practice at Rolls-Royce plc. The bars were ≈12.5 mm in diameter and ≈200 mm in length, Fig. 1. Post-processing steps that can induce strain, such as grit-blasting, were not employed. Several bars received a two-stage heat treatment at Bodycote plc. The first stage was a ramped solution heat treatment with a final step of ≈1315 °C for 6 h; the second stage primary age, was at 1140 °C for 6 h. Other bars remained in the as-cast state.

3.2. Sample preparation

The bars were sectioned lengthways, parallel to [001], with silicon carbide (SiC) blades, at the positions indicated in Fig. 1. The samples were mounted in conducting Bakelite, and ground with SiC paper from 1200 grit to 4000 grit. Final polishing was with a 3 μm diamond suspension (≈5 min), followed by a dilute 0.04 μm colloidal silica suspension (≈3 min).

A sample for transmission electron microscopy (TEM) was extracted from a specific location using the focussed-ion beam (FIB) technique in the Helios Nanolab 600 dual-beam field emission gun scanning electron microscope (FEGSEM). Sample preparation was done using standard techniques (technical details included in supplementary material) but the final stages of thinning at the lowest beam currents were not possible, consequently, some ion-beam damage was observed in the final microstructure.

3.3. Characterisation

Electron imaging with backscattered (BSE) and secondary electrons (SE), and energy dispersive x-ray spectroscopy (EDX) were performed on the CamScan MX2600 or JEOL 5800LV microscopes. Generally, imaging was done at 15 kV with a working distance of 10–15 mm, and the EDX data was acquired using Inca software from Oxford Instruments at 25 kV with either 35 mm (CamScan MX2600) or 10 mm (JEOL 5800LV) working distance.

The electron backscattered diffraction (EBSD) data was acquired at 25 kV with 30 mm working distance using the CamScan MX2600 FEGSEM and the CHANNEL 5 HKL software from Oxford Instruments. Orientation data is presented as inverse pole figures (IPF) and local misorientation maps (kernel method, 11 × 11 pixel matrix) acquired using 0.4–0.6 μm step size. Only misorientations ≥5° were considered, as misorientations of ≈3° were measured between adjacent dendrites.

Electron probe microanalysis (EPMA) was done using the Cameca SX100 microscope. The wavelength dispersive spectrometers used and the element spectral lines used are given in the supplementary information. The data was acquired at 20 kV with a 1 μm spot size and 40 nA current, and the acquisition time was 30 s except for Hf and Re, where 60 s was used due to weaker signals.

Transmission Electron Microscopy on the sample prepared by FIB was performed on a JEOL 200CX microscope operating at 200 kV.

3.4. Mechanical testing and annealing

Half-cylinder samples ≈12 mm in length were cut slowly with SiC blades from the as-cast bars to be deformed on an Instron 8800 servo-hydraulic low cycle fatigue machine. Fully heat-treated RR3010 was used as platen material. Samples were compressed at 0.2% min^{-1} along the [001] axis at room temperature to induce 3% plastic strain. To reduce friction with the platens carbon sheets and Cu grease were used.

To remove ≈100 μm of the surface, the deformed samples were electrolytically etched in a solution of 7 vol% perchloric acid in ethanol. This was done in an ice-bath at 15 V, and uniform etching was achieved at a rate of 5–10 μm min^{-1}. Although etching reduced nucleation from the damage caused by the platen, the depth was not sufficient to eliminate it altogether.

The etched and un-etched samples were sealed in fused silica tubes backfilled with Ar, and were given the standard solution heat treatment, with one sample interrupted after 30 min at 1315°. For examination, the polished surfaces were immersed in Kalling's etchant (10 gms $CuCl_2$ + 50 ml HCl + 50 ml ethanol) for 1–2 min to reveal the grain structure in the optical microscope.

4. Observations from the cast surface

The CMSX 4 bars are shown in the as-cast condition, Fig. 1a, and after the standard heat treatment, Fig. 1b. Almost 65% of the upper part of the as-cast bar has a shiny-silver colour (upper mould

[1] CMSX-4 is a registered Trade mark of the Cannon Muskegon Company.

Table 1
Chemical compositions (wt%) from EPMA of micro-grains and surface eutectic at positions A and B (see Fig. 1a), and eutectic in the bulk microstructure; standard deviations are given in parentheses.

		Ti	Ta	Al	Hf	Co	Cr	W	Re	Mo	Ni
Position A											
Nominal Alloy Composition		1.00	6.50	5.60	0.10	9.00	6.50	6.00	3.00	0.60	Bal.
Micro-grains		3.33 (0.48)	11.96 (0.79)	6.45 (0.38)	0.76 (0.47)	7.63 (0.19)	4.35 (0.94)	0.88 (0.34)	0.32 (0.08)	0.31 (0.06)	62.23 (1.20)
Surface eutectic	Interface with dendrites	1.66 (0.13)	10.48 (0.74)	6.97 (0.21)	0.13 (0.05)	7.65 (0.34)	3.76 (0.71)	2.47 (0.58)	0.58 (0.24)	0.26 (0.06)	65.51 (0.71)
	Interface with mould	3.59 (0.50)	11.52 (1.40)	6.42 (0.25)	1.10 (0.75)	7.71 (0.33)	3.83 (0.31)	0.53 (0.36)	0.17 (0.09)	0.23 (0.03)	62.28 (0.85)
Bulk eutectic		1.95 (0.24)	11.19 (0.77)	6.81 (0.15)	0.42 (0.43)	7.44 (0.31)	3.45 (0.53)	1.99 (0.53)	0.67 (0.29)	0.26 (0.06)	65.12 (0.58)
Position B											
Micro-grains		3.05 (0.76)	10.39 (2.66)	6.72 (0.75)	0.36 (0.09)	8.09 (1.21)	5.49 (4.11)	0.97 (0.47)	0.41 (0.38)	0.36 (0.34)	62.93 (3.37)
Surface eutectic	Interface with dendrites	1.98 (0.17)	10.99 (0.66)	7.17 (0.16)	0.27 (0.10)	7.51 (0.18)	3.50 (0.40)	1.96 (0.34)	0.36 (0.08)	0.20 (0.06)	65.30 (0.57)
	Interface with mould	2.85 (0.16)	11.74 (0.06)	6.95 (0.11)	0.38 (0.03)	7.51 (0.08)	3.67 (0.04)	1.13 (0.21)	0.26 (0.01)	0.22 (0.03)	63.76 (0.27)
Bulk eutectic		1.95 (0.24)	11.19 (0.77)	6.81 (0.15)	0.42 (0.43)	7.44 (0.31)	3.45 (0.53)	1.99 (0.53)	0.67 (0.29)	0.26 (0.06)	65.12 (0.58)

positions), characteristic of a layer of surface eutectic [25]. The lower part has a dull grey colour and does not show any surface eutectic.

In sections 4.1 and 4.2, the two types of casting surfaces are dealt with separately as the results show that the nucleation of recrystallisation at the surface is different in the two regions. Observations before and after solution heat treatment will be presented and discussed.

The results included in this paper are from a single bar, but are consistent with observations from many other bars. Finally, the effects on recrystallisation of removing the surface will be presented in section 5.

4.1. Micro-grains within the surface eutectic (upper mould positions)

4.1.1. As-cast condition

Fig. 2a shows a longitudinal section parallel to [001] at position A, Fig. 1a. The secondary dendrite arms do not reach the mould wall but are separated by a layer of surface eutectic. More significantly, Fig. 2b shows the corresponding inverse pole figure map, and distinct micro-grains are present within the surface eutectic. The bulk, and most of the surface eutectic, has a single orientation.

Lower in the casting at position B, close to the onset of the surface eutectic, similar micro-grains were observed but at a lower density within a thinner layer of surface eutectic, (Another example is included in supplementary material, Fig. 1). In the lower mould position, Fig. 1a, where no surface eutectic was present, no micro-grains were observed.

The angular misorientations of 40 micro-grains at positions A and B were measured with respect to the bulk single crystal, and show a large spread in misorientation angle, Fig. 3, with 90% of the grain boundaries having misorientations greater than 25°. Although 75% of micro-grains had misorientations less than 5° away from an ideal coincidence site lattice (CSL) misorientation with $\Sigma \leq 29$, none was disproportionately represented. Most of the micro-grains in the surface eutectic have high-angle boundaries with the bulk single crystal and are hence potential nuclei for recrystallisation in the presence of sufficient casting deformation.

The elemental distribution around the micro-grains is shown in Fig. 2c. Generally, the micro-grains had the same composition as the single-phase γ' surface eutectic, enriched in Ti, Ta and Al relative to the bulk, however, some composition variation did exist.

Higher magnification views of the micro-grains in Fig. 2c, together with other examples are shown in Fig. 4. Several other phases are associated with the surface eutectic whether or not micro-grains were present as reported by Leyland [28]. These fall into three categories with respect to composition. Phase a was Cr-rich with significant concentrations of Mo and Re, consistent with the σ phase identified by Mihalisin et al. [29]. Phase b was rich in Ta, W, Re, Mo and Cr, and phase c had a needle morphology rich in Al and Cr, with significant proportions of Ti. The number density of these phases increased with casting height.

Quantitative EPMA analyses of the compositions of the surface eutectic and micro-grains at bar heights A and B are presented in Table 1. The composition of the surface eutectic varied from the dendrite interface to the mould, and was enhanced in Ti, Cr and Hf at the mould surface. The composition of the micro-grains located

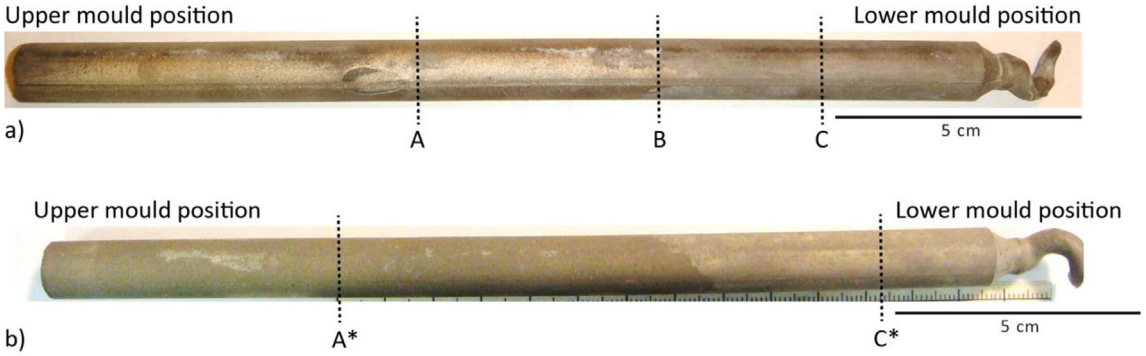

Fig. 1. CMSX 4 bar after a) foundry casting, and b) the standard heat treatment; positions examined are marked A for the region exhibiting surface scale and C for the region showing no surface scale: region B intersects both.

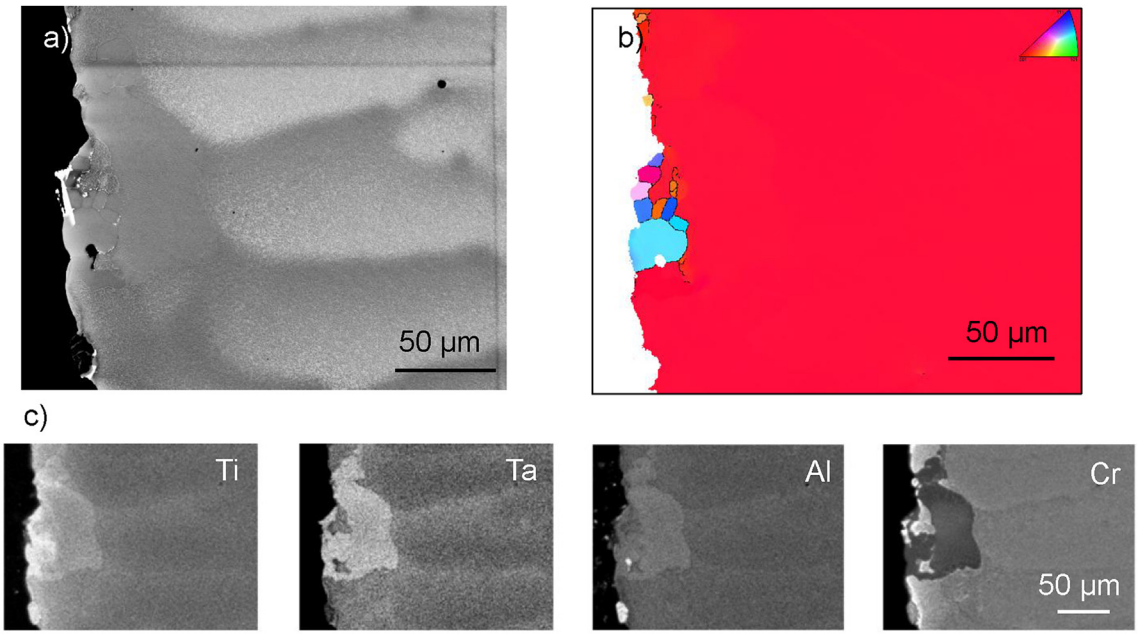

Fig. 2. Micro-grains in the surface eutectic at position A (see Fig. 1a); a) BSE image, b) EBSD-IPF and c) EDX maps.

at the mould surface was similar to the surrounding γ′. In CMSX 4, Ti segregated most strongly to the interdendritic liquid [30], and Cr segregated to the last solidifying liquid in the presence of eutectic γ′ [31]. The composition of surface eutectic nearest to the dendrites was similar to the eutectic found in the bulk of the casting.

Table 2 compares quantitative observations of the size and density of the micro-grains and surface eutectic made at bar positions A and B. The smallest micro-grains penetrated 2–3 μm from the casting surface, and the largest ones at positions A and B went deeper to ≈30 μm and ≈20 μm, respectively. This trend followed the average thickness of the surface eutectic, which was 50% thicker at upper position A. However, the average depth of the micro-grains was 12–15 μm and did not vary significantly with casting height. The micro-grains were elongated along the length of the bar, with an average aspect ratio of ≈3:2 at both positions.

At the lower casting height, position B, single micro-grains or clusters of 2–3 were observed at an average spacing of 1 mm, (see Fig. 2 in the supplementary material). At the higher position A, the occurrence of micro-grain clusters of up to 8 micro-grains, doubled to 2 per mm of casting surface, Table 2. The proportion of the cast surface covered by surface eutectic γ′ was ≈44% irrespective of casting height; however, the individual surface eutectic pools were fewer and longer at position A, consistent with the increased clustering of micro-grains at the higher casting height.

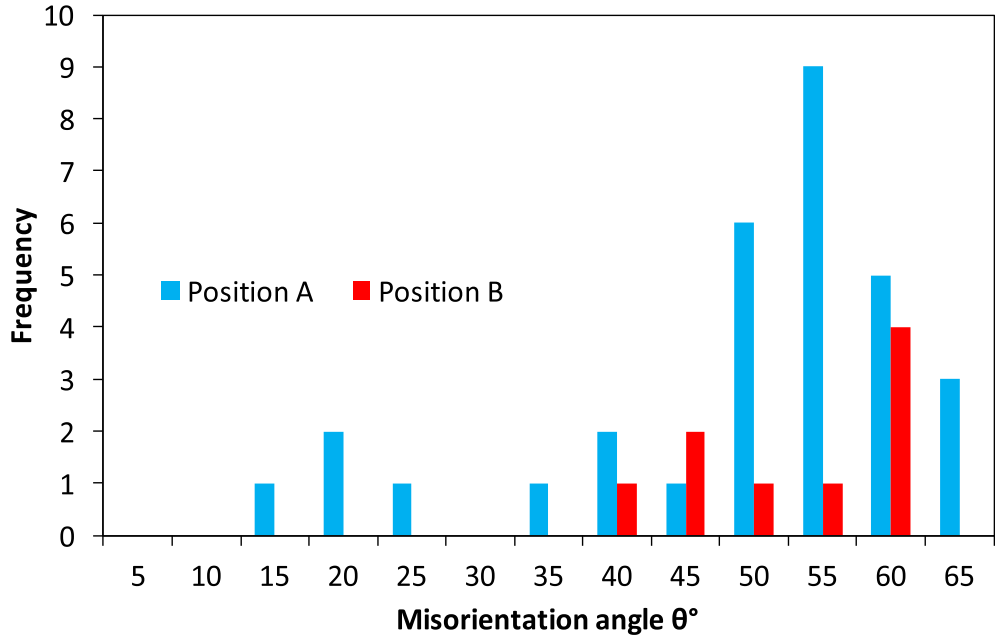

Fig. 3. Angular misorientation (θ) distribution of micro-grains in the surface eutectic with respect to the bulk single crystal.

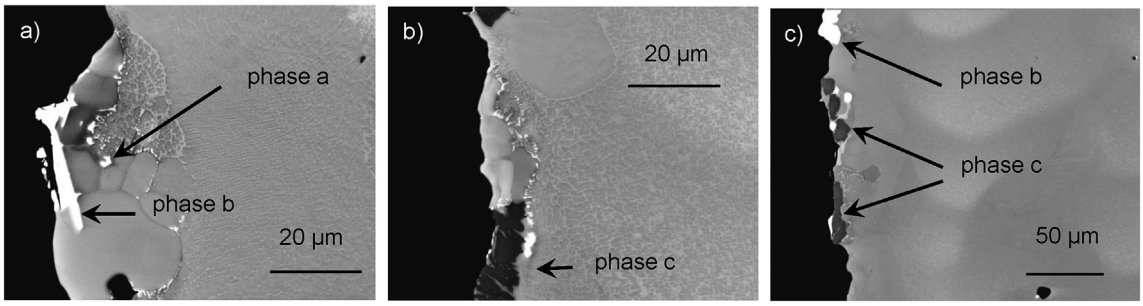

Fig. 4. Micro-grains in the surface eutectic at position A, a) detail from Fig. 2c, b) and c) show other examples.

Table 2
Observations of micro-grains and surface eutectic at positions A and B; *width measured from the surface.

		Position A	Position B
Micro-grains	*Average width (μm)	12.34 (2.96 < range < 29.92)	14.82 (2.25 < range < 21.56)
	No. of micro-grains (per mm of casting surface)	5	2
	No. of micro-grain clusters (per mm of casting surface)	2	1
Surface eutectic	*Average thickness of eutectic pools (μm)	30.40 (14.99 < range < 77.34)	19.43 (7.79 < range < 59.95)
	Average length of each eutectic pool (μm)	84.00	49.63
	Surface coverage of eutectic (%)	44.29	44.14

4.1.2. As heat-treated condition

The heat-treated bar was examined at position A*, equivalent to position A in the as-cast condition, Fig. 1. The longitudinal section parallel to [001] is shown in Fig. 5. The dendrites were no longer visible due to chemical homogenisation, and the inverse pole figure map from EBSD clearly shows that some of the micro-grains persisted after heat treatment. These were mostly single grains and were elongated parallel to the surface with an aspect ratio of 5:2. The density of the micro-grains reduced to 1 per mm, half that of the clusters in the as-cast condition at position A.

The histogram of angular misorientation from the bulk crystal of 21 micro-grains is given in Fig. 6. The number of micro-grains at position A* had halved relative to the as-cast bar at A. Misorientation angles with respect to the bar were between 27° and 60°. Some 50% of the boundaries were identified with CSL misorientations ($\Sigma \leq 29$ within 5°) but no particular misorientation was prominent. Some micro-grains were twin-related pairs.

Following the two-stage heat treatment, the surface eutectic had disappeared, but a segregated layer remained, richer in the interdendritic-partitioning elements Ti, Ta and Al, and depleted in Cr, Re and W, Fig. 5c. The micro-grains mostly remained single-phase γ', however, close to the grain boundary, γ had formed within the micro-grains, as the composition approached that of the bulk bar. Al enrichment at the surface is due to alumina formed

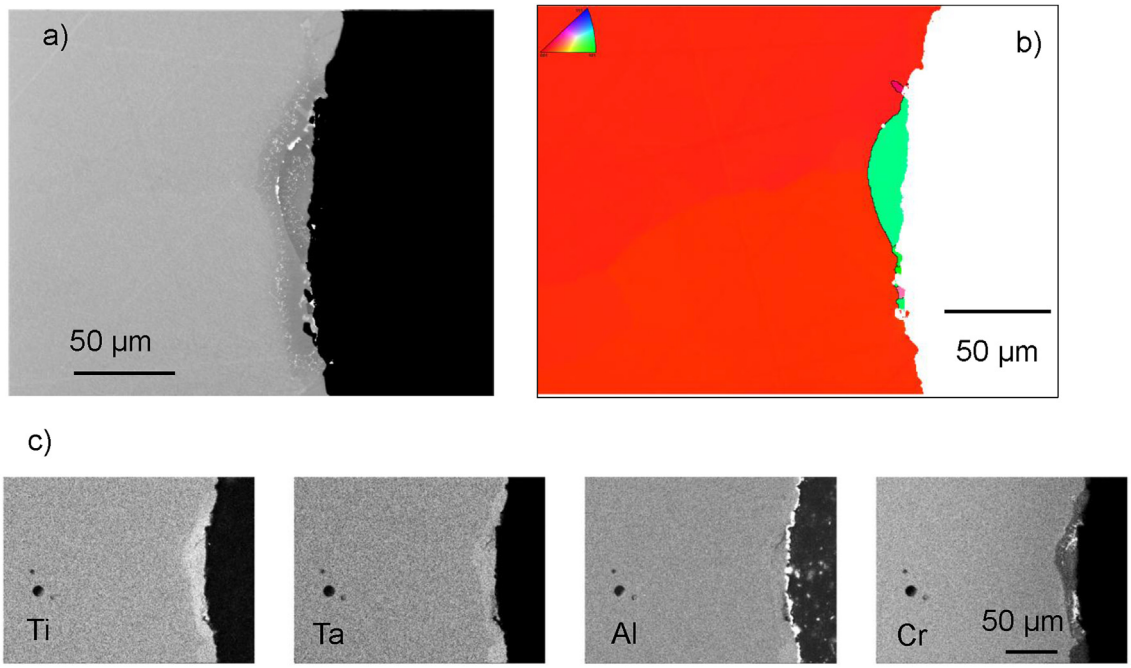

Fig. 5. Micro-grains on the surface at position A* after the heat treatment a) BSE image, b) EBSD-IPF and c) EDX maps.

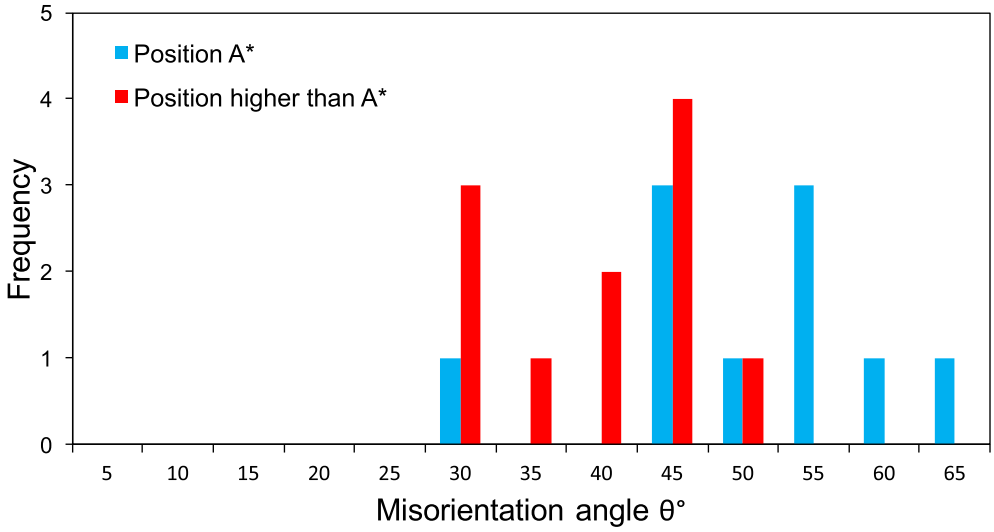

Fig. 6. Angular misorientation (θ) distribution of micro-grains with respect to the bulk single crystal after heat treatment.

during thermal exposure, Fig. 5c. Compositions of the bulk, surface layer and micrograins are given in supplementary material.

On the heat-treated surface, and on the grain boundaries, in addition to the phases a, b and c, present in the as-cast bar, topologically close packed (TCP) phases rich in W, Re, Mo and Cr were seen; phases rich in Hf and Ni were also observed. These phases were present on the grain boundaries and in other regions of the surface layer where no micro-grains existed, Fig. 7.

4.1.3. Discussion

The presence of the micro-grains of γ′ is clearly related to the surface eutectic. As the casting is withdrawn from the furnace and solidifies, partitioning causes a build-up of Ta, Ti and Al rich liquid ahead of the dendrites. The first dendrites to form at the base of the casting impinge on the mould wall during solidification and no surface eutectic is observed. The volume of segregated liquid builds to steady-state and is forced to the mould wall by the contraction of the higher dendrites as they solidify. This results in a semi-continuous eutectic layer at the mould wall in the upper part of the casting balanced by the characteristic loss of interdendritic liquid from the top of the casting revealing the dendrite arms. Brewster et al. [25,32] argue that this layer separates from the mould more easily on solidification and oxidises, resulting in a shiny-silver surface contrast seen in Fig. 1. The lower part of the bar remains in contact with the mould, surface eutectic is not formed and this area displays a dull-grey colour. During heat treatment alumina forms on the surface eutectic, which causes the change in surface contrast of the bar; hence the interference of visible light with different oxide thicknesses results in the rainbow colours seen in the upper part of the casting, Fig. 1, [20,25].

The micro-grains form in the surface eutectic in the upper part of the casting. Their composition resembles the surface eutectic closest to the mould surface, which, together with their position at the surface, suggests that whilst most of the eutectic solidifies with the same orientation as the bulk, small grains nucleate heterogeneously from the mould wall during the solidification of the interdendritic fluid. The frequency of occurrence of micro-grains appears to scale with the average size of the surface eutectic pools, being absent at the base and larger at the higher casting height.

The micro-grains observed in the surface eutectic resemble the freckle-chain defects observed in directionally cast alloys. Here we distinguish between the larger (mm-scale) grains resulting from the growth of dendrite fragments, which have the same composition as the single crystal bulk and form within the bulk, and the smaller chains of multiple grains (<1 μm) having a composition similar to the interdendritic liquid [33–37]. The latter freckles and the micro-grains described here, both form on the surface of the casting and have compositions similar to the interdendritic areas. It may be that freckles grow from similar micro-grains under suitable low thermal gradient and growth rate conditions. However, the CMSX 4 bar used in this study was cast under using process parameters optimised to minimise freckle formation during casting.

The micro-grains that form within the surface eutectic during casting are stable even after the heat treatment cycle: some grains grow substantially, but many smaller grains within clusters,

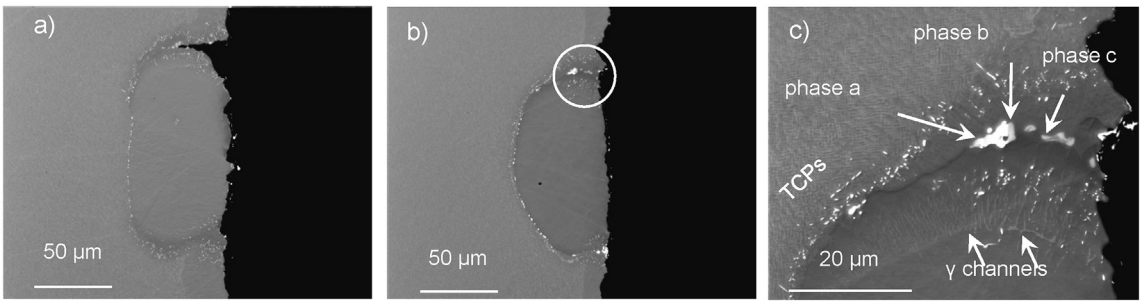

Fig. 7. a) and b) Micro-grains and the surface-segregated layer at position A* c) detail of the region highlighted in b).

disappear. Heat treatment causes significant homogenisation but the surface layer retains a distinct composition. This is closer to that of the bulk and a clear γ/γ' structure can be seen. The other precipitates at the boundaries dissolve during solution heat treatment, allowing unimpeded boundary migration, but re-precipitate at the boundary during cooling, principally as TCP phases. Hence, the micro-grains constitute potential recrystallisation nuclei, should sufficient dislocation density be present to drive migration.

4.2. Grain formation due to mould adherence (lower mould positions)

4.2.1. As-cast condition

In the lower part of the bar there is no surface eutectic, and no micro-grains. However, some particles from the mould wall adhere to the casting surface, Fig. 8a. Close to these adhered ceramic particles, regions of severe localised plastic deformation were found. This is quantified in Fig. 8b, which plots the relative misorientation between pixels using EBSD. The misorientation with respect to the bulk crystal accumulates towards the surface as shown by the profiles in Fig. 10c taken along the two lines indicated. Line profile 1 shows a gradual increase in misorientation reaching ≈13° at the casting surface; whereas for line profile 2, a sharp increase in misorientation is seen 10–15 μm from the casting surface with a maximum misorientation of 23°. Assessment of other sites of deformation showed misorientations of 5–10° for the most part, with some 10% of misorientations in excess of 15°, Fig. 8c. Most locally-deformed sites were 5–20 μm deep, although some were in excess of 50 μm.

A TEM sample was extracted from the region marked in Fig. 7b. The sample is a vertical radial section with the foil normal close to <100>. It retained some ion-beam damage after preparation. Distinct deformation bands cutting through the microstructure separate relatively dislocation-free regions 3–4 μm wide, Fig. 9. The diffraction patterns reveal a maximum of 5° in-plane rotation around <100> across the deformation bands. Additionally, an out-of-plane misorientation as high as 17.5° was observed between adjacent regions by tracking the rotation of the <100> pole on each side of the deformation band.

4.2.2. Heat-treated condition

After heat treatment the local surface deformation was sufficient to cause limited recrystallisation in the deformed regions. A longitudinal section along [001] at approximately position C* is shown in Fig. 10a. Another example is given in Fig. 3 of the supplementary material. The corresponding inverse pole figure map, Fig. 10b, shows the presence of small grains on the surface. Fig. 11 shows part of a continuous run of surface grains in excess of 5 mm in length.

Adjacent grains frequently showed Σ3 twin misorientations marked with a "T" in Fig. 10b. For each twin-related group, one grain showed a low misorientation angle, relative to the bulk, within the range of angular deviations seen in the as-cast bars due to local deformation. For example, in Fig. 10b, the grain with a misorientation of 16.5° formed a twin with a misorientation of 57°; this, in turn, formed another twin with a misorientation of 55°. A total of 39 grains from the heat-treated bar were analysed from position C*, Fig. 1b, together with 21 regions of high surface

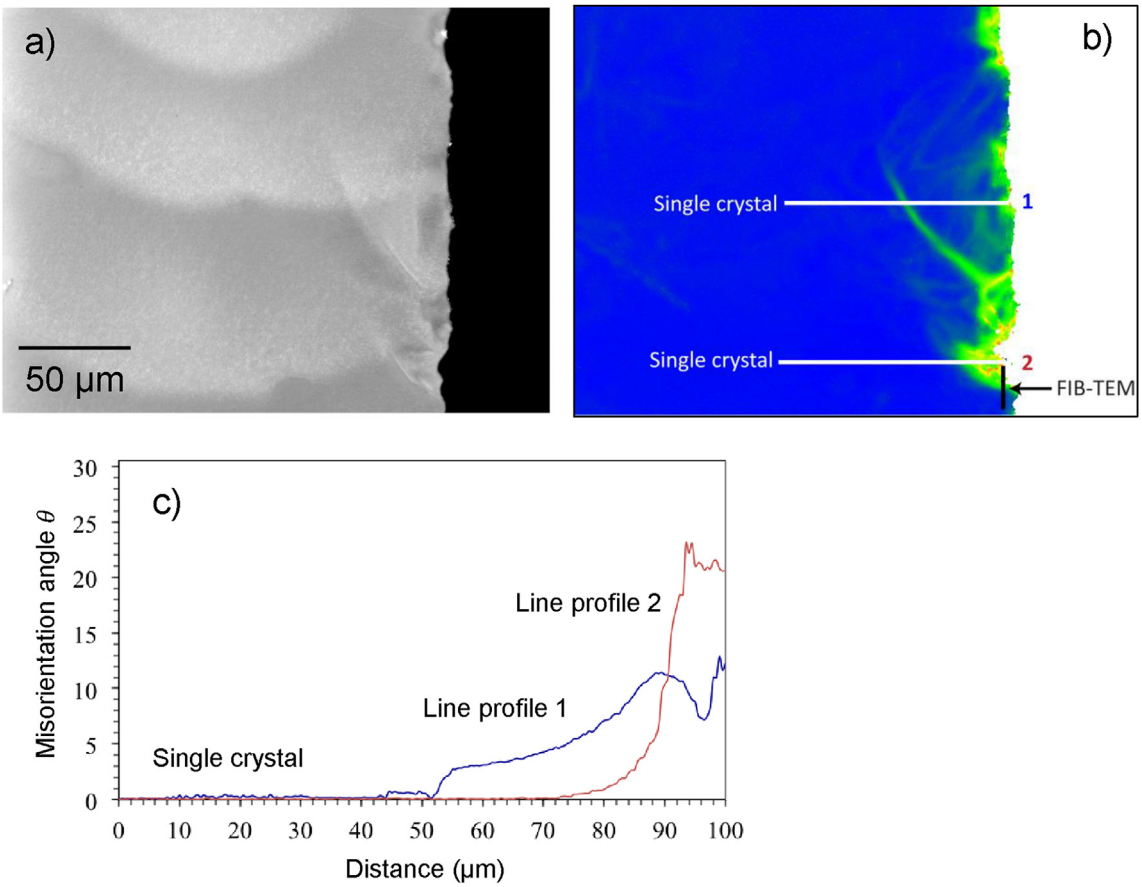

Fig. 8. Local surface strain accumulation at position C where the surface eutectic is absent. This is revealed by a) the contrast in the BSE image, and b) lattice rotations in the EBSD-local misorientation map; c) the angular misorientation profiles with respect to the bulk single crystal along lines 1 and 2 in b).

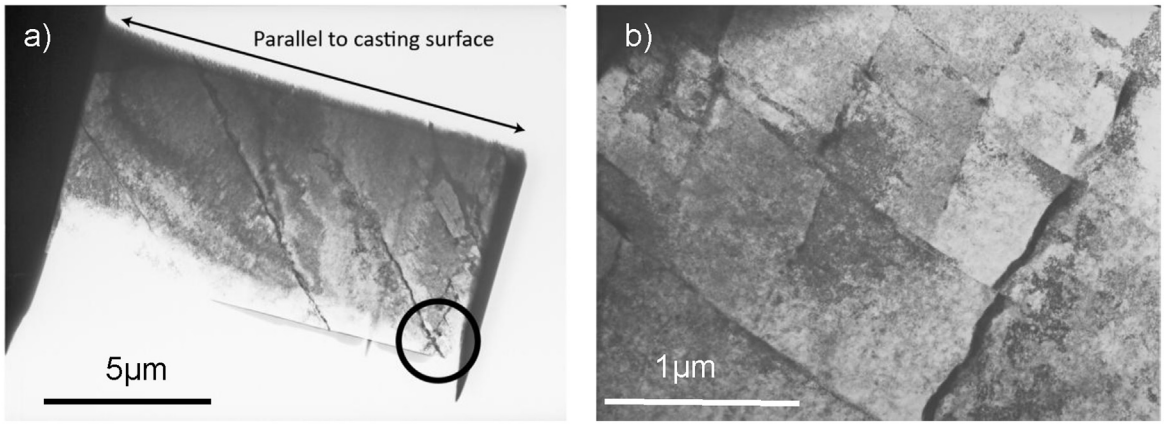

Fig. 9. TEM sample prepared using FIB from the region highlighted in Fig. 8b); a) shows the overall sample, and b) shows detail of the region circled in a); the foil normal is near [010].

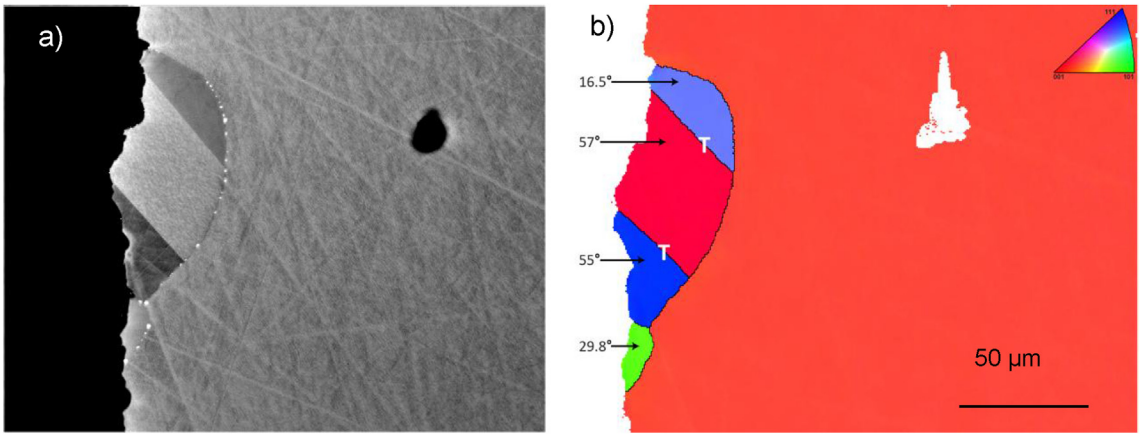

Fig. 10. Surface grains from recrystallisation at position C* after heat treatment; a) BSE image and b) EBSD-IPF map; twin boundaries (T) and the angular misorientations from the bulk single crystal are shown for each grain.

deformation from the as-cast bar at positions B and C. The misorientation angle distributions, Fig. 12, overlap closely in the lower angle range indicating that the rotations due to deformation (5–25°) are retained after heat treatment. The higher angle misorientations (>30°) were found only in the heat-treated bar and could always be traced back to the lower angle misorientations by one or more twin-related grains. Further examples are given in the additional material.

Fig. 11 shows further examples of surface grains after heat treatment. The fine γ/γ′ microstructure within the grains shows that grain formation occurred in the single-phase γ region during the solution heat treatment and γ′ precipitated on subsequent cooling consistent with the grain orientation, Fig. 11c. EDX analysis showed no composition differences between the grains and the bulk. On cooling from the heat treatment temperatures occasional TCP phases precipitated at the grain boundaries consistent with the slight instability of the bulk composition, Fig. 11c.

Most grains penetrated between 20 and 60 μm into the bulk, but some examples went as deep as ≈160 μm. In Fig. 11a, 4–5 grains formed along 1 mm of the surface; however elsewhere grains were continuous along the surface length examined (≈5 mm). No systematic variation with the solidification height within the lower

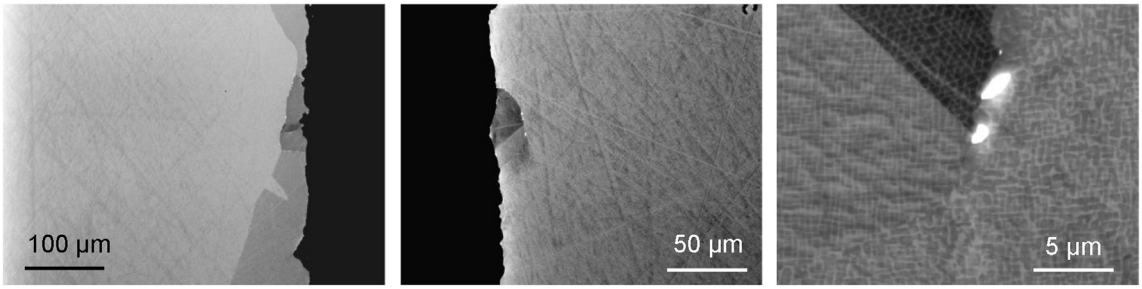

Fig. 11. Three examples of grains from surface recrystallisation at position C* after heat treatment; note TCP phases at interface.

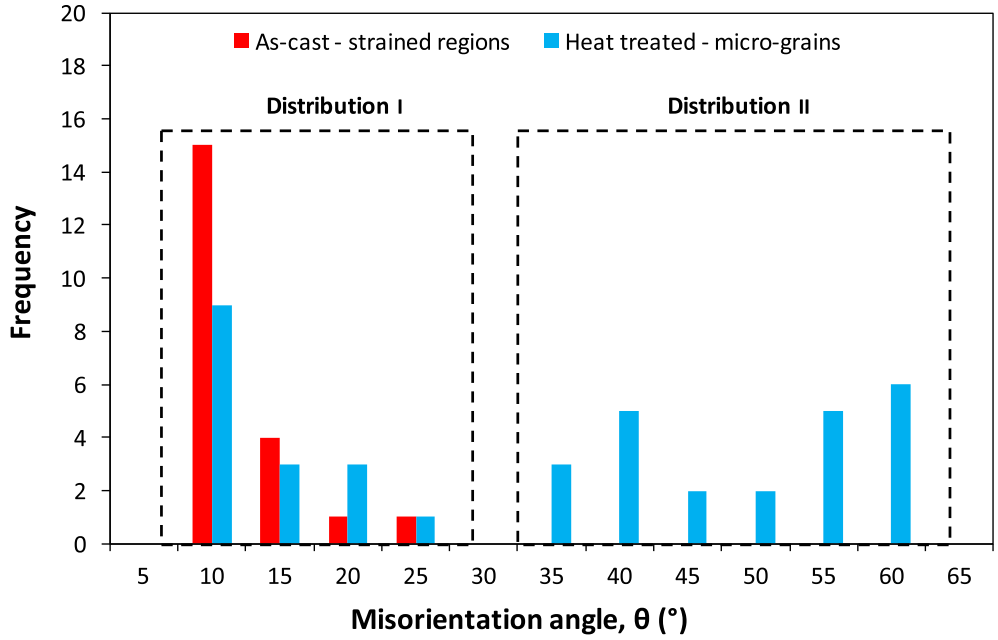

Fig. 12. Angular misorientation (θ) distribution of surface recrystallisation grains after heat treatment with respect to the bulk single crystal; maximum misorientations from strain accumulation in the as-cast condition are included in red. (For interpretation of the references to colour in this figure legend, the reader is referred to the web version of this article.)

half of the bar was observed.

4.2.3. Discussion

The strong association of severe local deformation with ceramic fragments attached to the surface suggests that deformation is caused as the mould becomes detached from the surface. The nature of the deformation revealed by the TEM (Fig. 9) as sharp localised slip bands is characteristic of deformation below 750 °C for superalloys [1,2]. This suggests that the damage is caused either during the later stages of cooling, or when the casting is separated from the mould after removal from the furnace; as observed by Li and Han [38]. The nature of the strong adherence of the mould in localised areas has been studied in detail by Brewster et al. [25].

Brewster et al. [25] argue that the bonding to the mould occurs via a reaction between the metal, specifically Al, and the silica in the mould leading to a jagged intrusive alumina which locks the casting to the mould. Detailed analysis of our material revealed a thin layer of alumina *beneath* the adhered ceramic consistent with their observations, (Fig. 4 in supplementary material). There is no evidence of mechanical locking caused by metal flowing into occasional small cavities and solidifying. Stresses to remove the ceramic, although low over the whole surface, become very high when concentrated on a small area, resulting in very high local deformation. These shearing stresses result in large accumulated misorientations with respect to the bulk in excess of 20°, but the increment of rotation is concentrated in narrow deformation bands that have a high proportion of geometrically necessary dislocations. Between these the material is relatively dislocation-free, and would become more so as the temperature is raised and the structure recovers. It is proposed that areas with the most extreme misorientations at the edge of the casting act as nuclei for the distinct grains that form during heat treatment. Low angle (~20°) grain boundaries develop from the shear bands, specifically at intersections, and accumulate misorientation as they absorb more shear bands until the dislocation density becomes too low to drive further growth. The correlation between misorientations measured in the as-cast sample and the lower-angle misorientations measured in the heat-treated material supports this interpretation.

From time to time, as is normal in recrystallisation of low stacking fault materials, faults occur behind the migrating boundary and twins form as a result [39–41]; up to second-generation of twinning was observed in this study. As the initial misorientation is low, the resulting grain will have a misorientation close to the 60° twin misorientation, but far enough away to avoid the sessile nature of the low energy facets of this boundary. Hence a wide range of high angle boundaries is seen, most of which are likely to be highly mobile. It is suggested that these act as the nuclei for recrystallisation in the lower parts of the casting where the internal casting stresses give rise to sufficient deformation to drive further migration as discussed in Panwisawas et al. [1,2].

5. Surface removal

Both mechanisms for the nucleation of recrystallisation described (§4.1, §4.2) are specific to the casting surface. Hence, if sufficient material were removed from the surface, recrystallisation could be controlled. To test this, bars were deformed 3% in compression to ensure sufficient driving force for recrystallsation and the effect of removing ≈100 μm from the as-cast surface was compared with complete bars after solution heat treatment.

Samples were taken from the upper part of the bars subject to surface eutectic. The convex surface and the vertical section parallel to [001] of the un-etched sample are shown in Fig. 13a–c after solution heat treatment, and reveal a fully recrystallised structure. The multiple grains highlighted on the convex surface originate from the cast surface, Fig. 13a, with the density of grains diminishing towards the centre of the vertical section in a columnar structure, Fig. 13b and c. The density of nuclei varies over the cast surface. Fig. 13d–f shows an un-etched sample fully recrystallised after only 30 min at the full solution heat treatment temperature.

In the fully heat-treated sample, Fig. 13a, 27 recrystallised grains over a surface area of ≈190 mm^2 were identified giving a density of 0.14 grains per mm^2. Based on the observed linear densities of 2 per mm at position A and 1 per mm at position B, §4.2, and assuming a random distribution of micro-grain sites in the as-cast material, it is estimated that 40–50 micro-grains per mm^2 were present in the

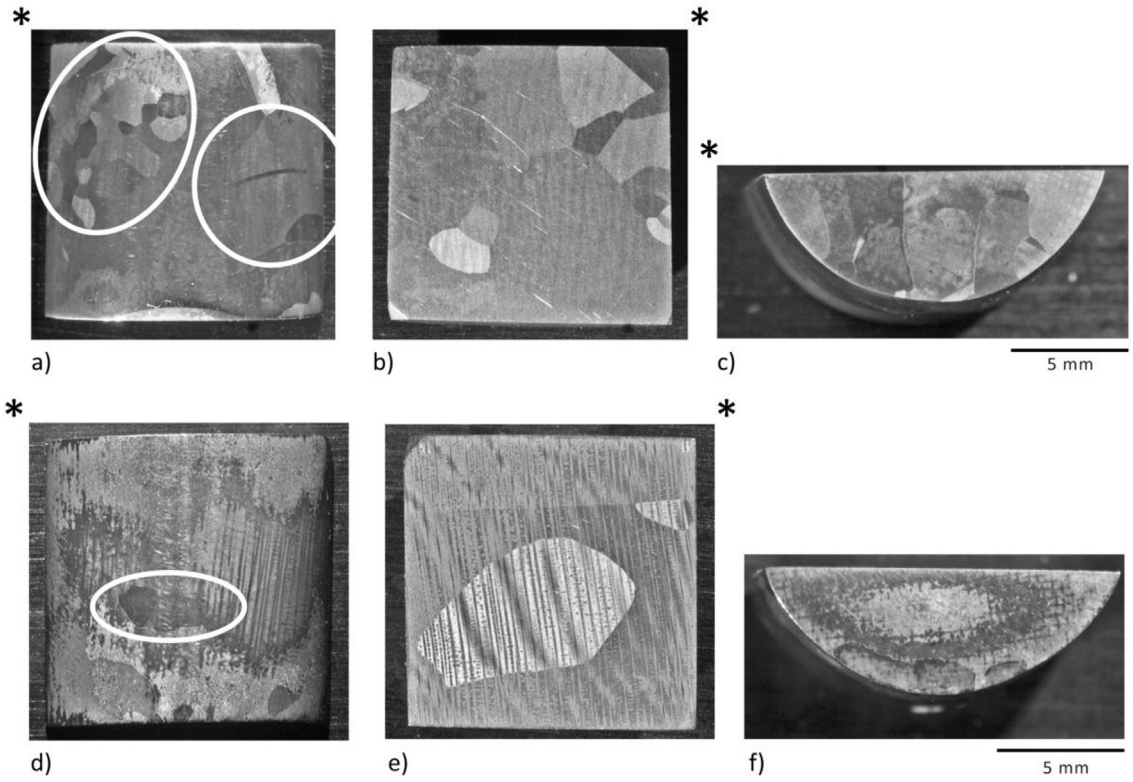

Fig. 13. Recrystallisation grains seen from a) the concave cast surface, b) the vertical section parallel to the deformation axis [001], and c) from one of the platen surfaces after the solution heat-treatment (nominal plastic strain of 3% at 20 °C was induced by compression along [001]); * marks the same corner in each view. All samples were fully recrystallised.

surface eutectic. Hence, between 1 in 300–350 of the micro-grain sites develops into a recrystallised grain.

The sample etched to a depth of 100 μm and solution heat treated remained, for the most part un-recrystallised, Fig. 14a. A few grains can be seen in the lower left corner and along the upper edge and most can be traced directly to the contact surface with the platen. The remaining three small grains half way up the left side of the convex surface are twins from the large grain growing from the platen-surface. The severe local strain accumulated at the platen-surfaces during deformation was not completely removed by the surface etching, and nucleated the few recrystallised grains observed which could be traced back, either directly or through a twin, to the platen surface. It is interesting that grains from the platen-surfaces did not to recrystallise the entire sample; this may be due to the lack of competition to produce high mobility interfaces, and competing recovery processes.

Results from these trials demonstrate that the micro-grains formed in the casting surface are the nuclei for recrystallisation and can grow in the presence of a sufficient dislocation density. Process modelling [1,2] has shown that in simple hollow geometries analogous to turbine blades a maximum plastic strain of 2–2.5% is induced during the casting process, and this has caused complete recrystallisation of such castings on subsequent solution heat treatment. Surface etching has been shown to suppress recrystallisation demonstrating that the degree of deformation sufficient to maintain recrystallisation cannot nucleate it.

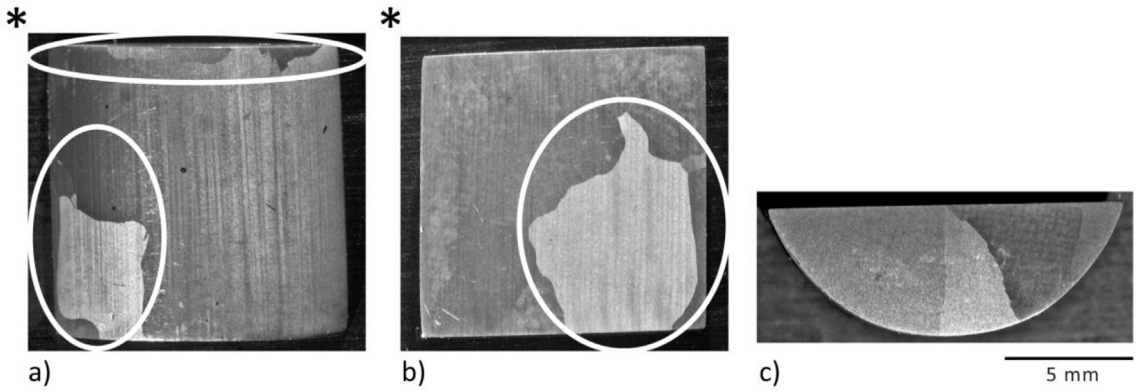

Fig. 14. Reduced recrystallisation in the etched sample seen from a) the concave surface, b) the vertical section parallel to [001], and c) from the lower platen surface after the full solution heat treatment (nominal plastic strain of 3% at 20 °C induced by compression along [001]); * shows the orientation between different views. Recrystallised areas are circled in Figures a) and b), all other areas are unrecrystallised.

Salkeld et al. [42] have patented surface etching as a method of suppressing recrystallisation after observing its beneficial effects in single crystal castings. The reason for the effectiveness of this process was not established, but the authors proposed that after casting a different strain-state exists on the surface. Their experimental trials on hollow aerofoil castings showed that removing as little as 13–50 μm of the surface significantly reduced recrystallisation. This depth is comparable to the defect size measured in this study and demonstrates that surface removal to this modest level can significantly reduce recrystallisation in single crystal castings.

Mihalisin et al. [29,43] demonstrated that carbon additions of up to 0.04 wt% substantially reduced the extent of surface eutectic formation and also the propensity for recrystallisation in single crystal castings. They proposed that carbides form preferentially from elements present in the surface eutectic and hinder the migration of recrystallisation grains. Tin et al. [36,37] provide a convincing explanation for the effectiveness of carbon in reducing freckle formation: carbides, which form just below the liquidus temperature, obstruct the flow of interdendritic liquid and reduce surface eutectic and surface freckle formation. This mechanism is consistent with the observations of Mihalisin et al. [29,43] and suggests that both recrystallisation and freckle formation are a result of the micro-grains formed at surface eutectic. However, carbon reduces the incipient melting temperature [44,45], making the solutioning of higher refractory-containing alloys more difficult; and deplete the substrate of elements such Ta and Mo.

Burgel et al. [17] report extensive work to mitigate surface-initiated recrystallisation in single crystal superalloys. Long anneals at low temperatures to promote recovery prior to solutioning failed to reduce recrystallisation. However, Bond and Martin [46], demonstrated that recovery treatments 100 °C below the solutioning temperature proved effective in eliminating recrystallisation after surface grit-blasting. It must be noted, however, that their straining conditions were significantly different from those used by Burgel et al. [17], who compressed samples at room temperature. Burgel et al. [17] observed that using surface aluminised coatings on as-cast single crystal samples substantially reduced the extent of recrystallisation. The process of aluminisation absorbs the outer layer of the casting in forming the aluminised layer [47], which is again consistent with nucleation from the surface grains. Surface coating is not a viable solution as it would need to be applied before solution heat treatment.

Surface etching, therefore, appears to be the best solution for mitigating recrystallisation in single crystal castings whether caused by cast-in micrograins or localised adhesion of the mould. Removing the casting surface by other mechanical means, such as grit-blasting or grinding, induces further surface strain that can cause recrystallisation. Etching can also produce components free from defects such as surface eutectic, surface contamination and melting. Abbott et al. [48] have demonstrated the use of electropolishing with ionic liquids to remove surface eutectic, and facilitate component examination for other grain defects. The existence of an effective and economic process to reduce recrystallisation would not only increase yield and reduce costs, but also allow the use of a wider range of alloys and more intricate blade designs.

6. Conclusions

Micro-grains of γ′ with high angle boundaries form within the surface eutectic towards the top of a casting.

The micro-grains survive the standard heat treatment even in the absence of a critical strain to produce recrystallisation.

In the lower part of the casing where surface eutectic is absent the metal can adhere to the mould locally; subsequent detachment creates locally deformed surface regions with rotations of up to 20° with respect to the bulk single crystal.

After heat treatment the deformed regions establish distinct grains by repeated twinning and have highly mobile misorientations with respect to the bulk.

Experimental trials demonstrated that, in the presence of a critical level of deformation in the bulk, etching the cast surface, can eliminate recrystallisation.

Acknowledgements

We are grateful to Drs. H.T. Pang and R.W. Broomfield for useful discussions; Drs. N. D'Souza, S.R. Irwin and B.R. Cooper for provision of materials; I. Buisman, D. Nicol, A.W. Rayment and K. Roberts for their generous assistance in the experimental work. H. Mathur and C. Panwisawas also thank Engineering and Physical Sciences Research Council and Rolls-Royce plc for financial support from Dorothy Hodgkin Postgraduate Awards and the EPRSC-Rolls-Royce Strategic Partnership Grant EP/H500375/1.

Appendix A. Supplementary data

Supplementary data related to this article can be found at http://dx.doi.org/10.1016/j.actamat.2017.02.058.

References

[1] C. Panwisawas, H. Mathur, J.-C. Gebelin, D.C. Putman, C.M.F. Rae, R.C. Reed, Prediction of recrystallization in investment cast single-crystal superalloys, Acta Mater. 61 (2013) 51–66.
[2] C. Panwisawas, H. Mathur, J.-C. Gebelin, D.C. Putman, P. Withey, N. Warnken, C.M.F. Rae, R.C. Reed, Prediction of plastic strain for recrystallisation during investment casting of single crystal superalloys, in: E. Huron, et al. (Eds.), Superalloys 2012, TMS: Seven Springs, Champion, PA, 2012, pp. 547–556.
[3] D.C. Cox, B. Roebuck, C.M.F. Rae, R.C. Reed, Recrystallisation of single crystal superalloy CMSX-4, Mater. Sci. Technol. 19 (2003) 440–446.
[4] R.M. Boothby, G.B. Merrill, N. Hansen, et al. (Eds.), 7th Riso International Symposium, Riso National Laboratory, Roskilde, Denmark, 1986, pp. 241–246.
[5] A.J. Porter, B. Ralph, The recrystallization of nickel-base superalloys, J. Mater. Sci. 16 (1981) 707–713.
[6] M. Dahlen, L. Winberg, The influence of γ′-precipitation on the recrystallization of a nickel base superalloy, Acta Metall. 28 (1980) 41–50.
[7] L. Wang, F. Pyczak, J. Zhang, L.H. Lou, R.F. Singer, Effect of eutectics on plastic deformation and subsequent recrystallization in the single crystal nickel base superalloy CMSX-4, Mater. Sci. Eng. 532A (2012) 487–492.
[8] L. Wang, F. Pyczak, J. Zhang, R.F. Singer, On the role of eutectics during recrystallization in a single crystal nickel-base superalloy – CMSX-4, Int. J. Mater. Res. 100 (2009) 1046–1051.
[9] M.M. Chaudhri, Subsurface plastic strain distribution around spherical indentations in metals, Philos. Mag. 74A (1996) 1213–1224.
[10] H.N. Mathur, C.N. Jones, C.M.F. Rae, A study on the effect of composition, and the mechanisms of recrystallisation in single crystal Ni-based superalloys, in: MATEC Web of Conferences 14, 07003, 2014, http://dx.doi.org/10.1051/matecconf/20141407003.
[11] L. Zhonglin, X. Qingyan, L. Baicheng, Microstructure simulation on recrystallization of an as-cast nickel based single crystal superalloy, Comp. Mater. Sci. 107 (2015) 122–133.
[12] L. Zhonglin, X. Qingyan, L. Baicheng, Simulation and experimental study of recrystallization kinetics of nickel based single crystal superalloys, in: Materials Today: Proceedings 2S, 2015, pp. S440–S452.
[13] L. Zhonglin, X. Jichun, X. Qingyan, L. Jiarong, L. Baicheng, Deformation and recrystallization of single crystal nickel-based superalloys during investment casting, J. Mater. Process. Technol. 217 (2015), 1–1.
[14] L. Wang, G. Xie, J. Zhang, L.H. Lou, On the role of carbides during the recrystallization of a directionally solidified nickel-base superalloy, Scr. Mater. 55 (2006) 457–460.
[15] J.X. Zhang, H. Harada, Y. Ro, Y. Koizumi, Superior thermo-mechanical fatigue property of a superalloy due to its heterogeneous microstructure, Scr. Mater. 55 (2006) 731–734.
[16] J.J. Moverare, S. Johansson, R.C. Reed, Deformation and damage mechanisms during thermal–mechanical fatigue of a single-crystal superalloy, Acta Mater. 57 (2009) 2266–2276.
[17] R. Burgel, P. Portella, J. Preuhs, Recrystallization in single crystals of nickel base superalloys, in: T.M. Pollock, et al. (Eds.), Superalloys 2000, TMS, Seven Springs, Champion, PA, 2000, pp. 229–238.
[18] Q.Z. Chen, C.N. Jones, D.M. Knowles, The grain boundary microstructures of the base and modified RR 2072 bicrystal superalloys and their effects on the creep properties, Mater. Sci. Eng. 385A (2004) 402–418.

[19] G. Xie, L. Wang, J. Zhang, L.H. Lou, Influence of recrystallization on the high-temperature properties of a directionally solidified Ni-base superalloy, Metall. Mater. Trans. 39A (2008) 206–210.
[20] G. Xie, L. Wang, J. Zhang, L.H. Lou, Intermediate temperature creep of directionally solidified Ni-based superalloy containing local recrystallization, Mater. Sci. Eng. 528A (2011) 3062–3068.
[21] G. Xie, L. Wang, J. Zhang, L.H. Lou, High temperature creep of directionally solidified ni base superalloys containing local recrystallization, in: R.C. Reed, et al. (Eds.), Superalloys 2008, TMS: Seven Springs, Champion, PA, 2008, pp. 453–460.
[22] B. Zhang, X. Lu, D. Liu, C. Tao, Influence of recrystallization on high-temperature stress rupture property and fracture behavior of single crystal superalloy, Mater. Sci. Eng. 551A (2012) 149–153.
[23] M. Okazaki, T. Hiura, T. Suzuki, Effect of local cellular transformation on fatigue small crack growth in CMSX-4 and CMSX-2 at high temperature, in: T.M. Pollock, et al. (Eds.), Superalloys 2000, TMS: Seven Springs, Champion, PA, 2000, pp. 505–514.
[24] U. Paul, P.R. Sahm, D. Goldschmidt, Inhomogeneities in single-crystal components, Mater. Sci. Eng. 173A (1993) 49–54.
[25] G. Brewster, H.B. Dong, N.R. Green, N. D'Souza, Surface segregation during directional solidification of Ni-base superalloys, Metall. Mater. Trans. 39B (2008) 87–93.
[26] A.D. Hill, Critical Strain for Recrystallisation in Single Crystal Alloys, Report for Rolls-Royce plc, Bristol, 1995.
[27] L. Zhonglin, F. Xiangyu, X. Qingyan, L. Baicheng, Influence of deformation temperature on recrystallization in a Ni-based single crystal superalloy, Mater. Lett. 160 (2015) 318–322.
[28] S.P. Leyland, I.M. Edmonds, S. Irwin, C.N. Jones, A. Bhowmik, D. Ford, C.M.F. Rae, The distribution and retention of yttrium and lanthanum in cast single crystal superalloys, in: M. Hardy, et al. (Eds.), Superalloys 2016, TMS: Seven Springs, Champion, PA, 2016, pp. 247–256.
[29] J.R. Mihalisin, J. Corrigan, M. Launsbach, E. Leonard, R. Baker, B. Griffin, Some effects of carbon in the production of single crystal superalloy castings, in: K.A. Green, et al. (Eds.), Superalloys 2004, TMS: Seven Springs, Champion, PA, 2004, pp. 795–800.
[30] R.A. Hobbs, S. Tin, C.M.F. Rae, A castability model based on elemental solid-liquid partitioning in advanced nickel-base single-crystal superalloys, Metall. Mater. Trans. 36A (2005) 2761–2773.
[31] H.T. Pang, L.J. Zhang, R.A. Hobbs, H.J. Stone, C.M.F. Rae, Solution heat treatment optimization of fourth-generation single-crystal nickel-base superalloys, Metall. Mater. Trans. 43A (2012) 3264–3282.
[32] G. Brewster, N. D'Souza, K.S. Ryder, S. Simmonds, H.B. Dong, Mechanism for formation of surface scale during directional solidification of Ni-base superalloys, Metall. Mater. Trans. 43A (2012) 1288–1302.
[33] A.F. Giamei, B.H. Kear, On the nature of freckles in nickel base superalloys, Metall. Trans. 1 (1970) 2185–2192.
[34] T.M. Pollock, W.H. Murphy, The breakdown of single-crystal solidification in high refractory nickel-base alloys, Metall. Mater. Trans. 27A (1996) 1081–1094.
[35] T.M. Pollock, W.H. Murphy, E.H. Goldman, D.L. Uram, J.S. Tu, Grain defect formation during directional solidification of nickel base single crystals, in: S.D. Antolovich, et al. (Eds.), Superalloys 1992, TMS: Seven Springs, Champion, PA, 1992, pp. 125–134.
[36] S. Tin, T.M. Pollock, W.T. King, Carbon additions and grain defect formation in high refractory nickel-base single crystal superalloys, in: T.M. Pollock, et al. (Eds.), Superalloys 2000, TMS: Seven Springs, Champion, PA, 2000, pp. 201–210.
[37] S. Tin, T.M. Pollock, W. Murphy, Stabilization of thermosolutal convective instabilities in Ni-based single-crystal superalloys: carbon additions and freckle formation, Metall. Mater. Trans. 32A (2001) 1743–1753.
[38] Y. Li, Y. Han, Recrystallization of Ni3Al base single crystal alloy IC6SX with different surface mechanical processes, J. Mater. Sci. Technol. 26 (2010) 883–888.
[39] H. Gleiter, The formation of annealing twins, Acta Metall. 17 (1969) 1421–1428.
[40] C.M.F. Rae, C.R.M. Grovenor, K.M. Knowles, Multiple twinning and recrystallisation, Z. fur Met. 72 (1981) 798–802.
[41] S. Mahajan, C.S. Pande, M.A. Imam, B.B. Rath, Formation of annealing twins in f.c.c. crystals, Acta Mater. 45 (1997) 2633–2638.
[42] R.W. Salkeld, T.T. Field, E.A. Ault, Preparation of single crystal superalloys for post-casting heat treatment (patent number 5,413,648). United Technologies Corporation: United States of America (1995).
[43] J.R. Mihalisin, J. Corrigan, G.M. Gratti, R.G. Vogt, Casting of single crystal superalloy articles with reduced eutectic scale and grain recrystallization (patent number US 2002/0007877 A1). United States of America (2002).
[44] S. Tin, L.J. Zhang, R.A. Hobbs, A.-C. Yeh, C.M.F. Rae, B. Broomfield, Linking the properties, processing and chemistry of advanced single crystal ni-base superalloys, in: R.C. Reed, et al. (Eds.), Superalloys 2008, TMS: Seven Springs, Champion, PA, 2008, pp. 81–90.
[45] M. Gell, D.N. Duhl, A.F. Giamei, The development of single crystal superalloy turbine blades, in: J.K. Tien, et al. (Eds.), Superalloys 1980, TMS: Seven Springs, Champion, PA, 1980, pp. 205–214.
[46] S.D. Bond, J.W. Martin, Surface recrystallization in a single crystal nickel-based superalloy, J. Mater. Sci. 19 (1984) 3867–3872.
[47] C.M.F. Rae, M.S. Hook, R.C. Reed, On the precipitation of topological close packed phases at aluminide coatings on superalloys and the effect of precipitate morphology, Mater. Sci. Eng. 396A (2005) 231–239.
[48] A.P. Abbott, N. D'Souza, P. Withey, K.S. Ryder, Electrolytic processing of superalloy aerospace castings using choline chloride-based ionic liquids, Trans. IMF 90 (2012) 9–14.